

Estimation and Spatiotemporal Variation Analysis of Net Primary Productivity in the Upper Luanhe River Basin in China From 2001 to 2017 Combining With a Downscaling Method

Qinru Liu, Liang Zhao , Rui Sun , Tao Yu, Shun Cheng, Mengjia Wang, Anran Zhu, and Qi Li

Abstract—The upper Luanhe River Basin is a significant ecological barrier guarding the Beijing–Tianjin–Hebei region in China. Quantitative measures of vegetation productivity can be used to assess ecosystem carbon sequestration capacity and monitor regional ecological environmental health. Although several vegetation productivity products have been generated, poor spatiotemporal resolution limits their application in ecosystem service assessment. In this article, vegetation net primary productivity (NPP) from 2000 to 2017 with a resolution of 30 m in the upper Luanhe River Basin was generated based on a data fusion model and the multisource data synergized quantitative (MuSyQ) NPP model. Then, the variation trend of NPP and its climate controls were analyzed. Compared with forest NPP observation data, we derived an R^2 of 0.68 and the root-mean-square error of $81.70 \text{ gC}\cdot\text{m}^{-2}\cdot\text{yr}^{-1}$. Annual NPP had a fluctuating increasing trend from 2001 to 2017, with values ranging between 3.43 and $5.00 \text{ TgC}\cdot\text{yr}^{-1}$, with an annual increase trend of $0.04 \text{ TgC}\cdot\text{yr}^{-1}$. Precipitation was significantly correlated with NPP in the upper part of the Luanhe River basin, which is an important reason for the interannual variation of NPP. Grassland had a stronger correlation to precipitation than forest because it is more sensitive to precipitation. The area where the temperature is significantly correlated with annual NPP only accounts for 2% of the study area, indicating that temperature has a weak influence on NPP. Furthermore, human activities, such as forest management, fertilization, and irrigation, can change the trend of annual NPP.

Index Terms—Climate controls, downscaling, net primary productivity (NPP), spatiotemporal variation, the upper Luanhe River basin.

Manuscript received July 8, 2021; revised October 20, 2021 and November 29, 2021; accepted November 29, 2021. Date of publication December 6, 2021; date of current version December 29, 2021. This work was supported by the National Key R&D Program of China under Grants 2017YFA0603002 and 2016YFB0501502 and in part by the National Natural Science Foundation of China under Grant 41531174. (*Corresponding author: Rui Sun.*)

Qinru Liu, Liang Zhao, Rui Sun, Mengjia Wang, Anran Zhu, and Qi Li are with the State Key Laboratory of Remote Sensing Science, Faculty of Geographical Science, Beijing Normal University, Beijing 100875, China, and also with the Beijing Engineering Research Center of Global Land Remote Sensing Products, Faculty of Geographical Science, Beijing Normal University, Beijing 100875, China (e-mail: liuqinru1105@163.com; zhaoliang@mail.bnu.edu.cn; sunrui@bnu.edu.cn; wmeng_jia@163.com; 452919047@qq.com; 201821051085@mail.bnu.edu.cn).

Tao Yu is with the Research Institute of Forest Resource Information Techniques, Chinese Academy of Forestry, Beijing 100091, China (e-mail: yutao-gis@ifrit.ac.cn).

Shun Cheng is with the Saihanba Machine Forest Center, Chengde 068450, China (e-mail: chshaaaa@163.com).

This article has supplementary downloadable material available at <https://doi.org/10.1109/JSTARS.2021.3132723>, provided by the authors.

Digital Object Identifier 10.1109/JSTARS.2021.3132723

I. INTRODUCTION

VEGETATION productivity is a key indicator for estimating carbon sequestration and characterizing vegetation activity, which plays a key role in climate change and the carbon balance [1]–[3]. Net primary productivity (NPP) indicates the efficiency of fixation and transformation of photosynthates and directly reflects productive capacity of vegetation in the natural environment [4]. Since the 1960s, NPP has been listed as one of the key issues in the International Geosphere–Biosphere Program, International Biology Plans, World Climate Research Programme, and Kyoto Protocol [5].

In situ observations provide a way to obtain vegetation productivity with high precision; however, they require large investments in finance and time and are limited to site-scale research [6]. Satellite remote sensing can supply large-scale land surface parameters data and many models based on remote sensing data have been developed to generate regional and global vegetation productivity products. The light-use efficiency (LUE) models that estimate gross primary productivity (GPP) or NPP from absorbed photosynthetically active radiation (PAR) and LUE are the most used models, such as the Carnegie–Ames–Stanford–Approach (CASA) [7], the GLObal Production Efficiency Model (GLO-PEM) [8], the Moderate Resolution Imaging Spectroradiometer (MODIS) NPP algorithm (MOD17) [9], the eddy covariance–light use efficiency model (EC-LUE) [10], and vegetation photosynthesis model [11]. The MOD17 GPP/NPP products have become the most generally used productivity products, and the spatial resolution is 500 or 1000 m [12]. However, the relatively coarse spatial resolutions of vegetation productivity products have restricted their application in ecosystem service and vegetation dynamic research at a local scale [13], [14]. In this context, utilizing the advantages of remote sensing data at different scales to produce high spatiotemporal resolution vegetation productivity and analyzing its spatiotemporal pattern is of prime importance to regional carbon budget assessment and ecological environmental monitoring.

Interannual variation of vegetation productivity is mainly influenced by climate and human activity. There have been efforts to study the impact of climate change on vegetation productivity in northern China [15]–[18]. Recent studies have shown that NPP in northern China has been increasing since this century,

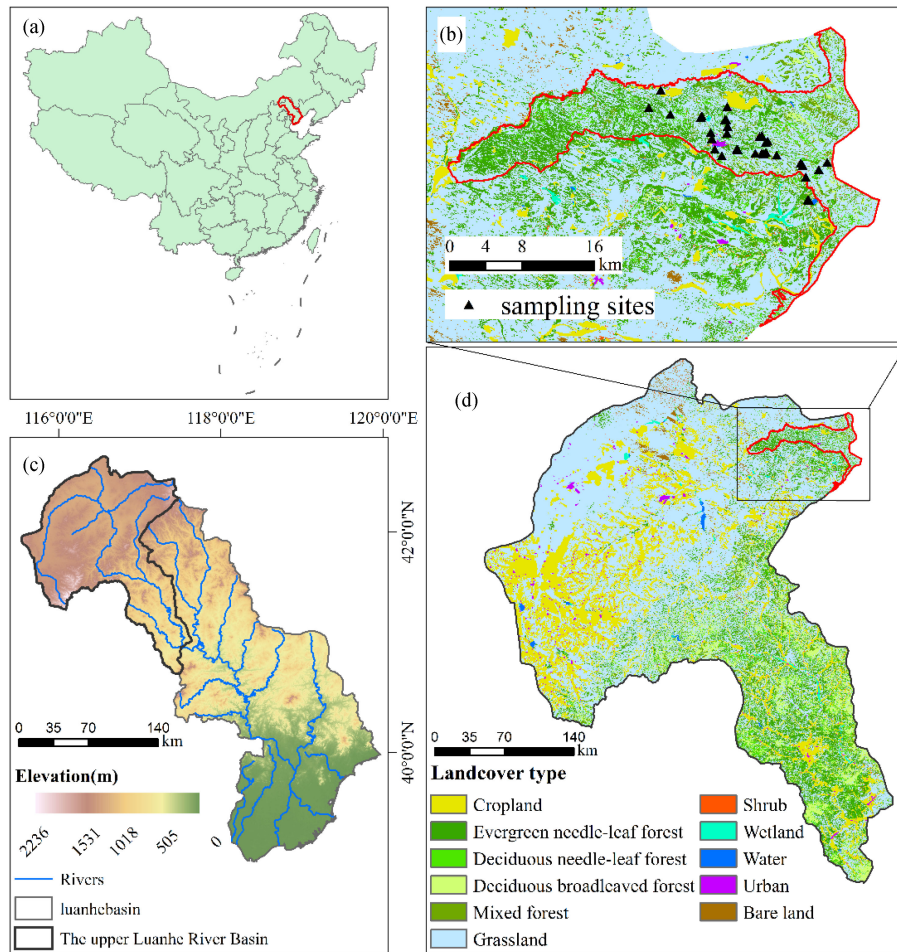


Fig. 1. (a) Location of the Luan River Basin. (b) Location of the Saihanba Forest Farm. (c) Altitude of the Luan River Basin. (d) Distribution of land-cover types in the upper Luanhe River basin.

and precipitation is the primary climatic factor for NPP growth, but temperature has an inhibitory effect on vegetation growth in these areas [16], [19], [20]. However, these findings are aimed at the overall trend of northern China or northern grassland.

The upper Luanhe River Basin is located in the arid/humid transition zone, which is also the transition zone from grassland to forest. It is a significant ecological barrier for guarding the Beijing–Tianjin–Hebei region in China, and its northern part is the core part of the “Three North Shelter Forest Project” and the “Saihanba Mechanical Forest Farm.” Since the 1960s, the Saihanba Forest Farm has responded to the national appeal for afforestation work to improve the ecological environment. Currently, Saihanba is home to the largest North China larch plantation in the Northern Hemisphere [21], as well as a large area of scotch pine plantation, which plays a key role in water conservation and climate regulation in the Beijing–Tianjin–Hebei region. Man-made or natural reshaping of the landscape occurs frequently, causing the vegetation growth to be very unstable, and the grassland is more sensitive to climatic change than the forest [17], [22], [23], which cause vegetation in the arid/humid transition zone to be more sensitive to climate fluctuations [18], [24]. Therefore, the response of NPP to the climate in this region remains uncertain.

The main purposes of this article are as follows:

- 1) to present a high-resolution of the leaf area index (LAI) and fraction of photosynthetically active radiation (FPAR) using a downscaling method;
- 2) to obtain high-resolution time series of GPP/NPP based on an LUE-based NPP model; and
- 3) to analyze the spatiotemporal variation and climate controls of NPP in the upper Luanhe River Basin.

This article provides a reference for the estimation of regional vegetation productivity with high resolution and helps reveal the ecological status of the upper Luanhe River Basin.

II. STUDY AREA AND MATERIALS

A. Study Area

The upper Luanhe River catchment is mainly located in the northern part of Hebei Province, China, bordering the Keshiketeng Banner of Inner Mongolia to the north ($40^{\circ}42'N$ – $42^{\circ}45'N$, $115^{\circ}36'E$ – $117^{\circ}36'E$). The location and land-cover types of the catchment are shown in Fig. 1. Land-cover types mainly are forest, cropland, grassland, bare land, and shrubs. The terrain descends from the northwest to the southeast, with

an altitude of 400–2300 m. The study area has a semiarid continental monsoon climate, with a temperature below 0°C in winter and approximately 20°C in summer and average annual precipitation of approximately 400 mm. The Saihanba National Nature Reserve in the northeastern part of the catchment is a typical forest-steppe ecotone ecosystem and was awarded “Champions of the Earth” from the United Nations Environment Program in 2017. The reserve has diverse ecological landscapes and rich biological species is one of the typical representative areas of vegetation in northern China. The tree species in the reserve mainly include North China larch, scotch pine, birch, and aspen.

B. Data and Data Processing

1) *Remote Sensing Data*: Global Land Surface Satellite (GLASS) LAI/FPAR products from 2001 to 2017 were published by the Center for Global Change Data Processing and Analysis of Beijing Normal University¹ with spatiotemporal resolutions 1 km/500 m and 8 days, respectively [25]–[28]. The Surface reflectance products came from the atmospherically corrected Landsat data of the United States Geological Survey.² This work collected 60 scenes of TM images and 42 scenes of ETM+ images from 2001 to 2017. Land-cover data adopted GlobeLand30 land-cover map for 2010, which was mapped from Landsat and Chinese HJ-1 satellite images, depend on the pixel-object-knowledge classification method. With spatial resolution of 30 m and overall accuracy of 83.5%, the map was composed of ten land-cover types, for example, forest, grassland, and cultivated land [29]. However, since the forest classification of GlobeLand30 was not refined, the forests in the study area were further classified into four types, i.e., deciduous needle-leaf forest, evergreen needle-leaf forest, deciduous broadleaved forest, and mixed forest, using a 30-m resolution forest map in China [30].

2) *Meteorological Data*: Meteorological data (daily maximum temperature, minimum temperature, mean temperature, and precipitation) gathered from 17 meteorological stations around the catchment were mapped to 30 m adopting the kriging interpolation. Monthly average temperature and precipitation were calculated from daily temperature and precipitation. In addition, the mountain microclimate simulation model (MT-CLIM) was used to simulate monthly solar shortwave radiation with a resolution of 30 m [31].

3) *Field Data*: Ground-based field data were collected at 32 plots in September 2017 and July 2018 in Saihanba, Hebei Province, China. According to the typical forest species, forest ages, and fraction of vegetation cover, 11 sample plots of *Pinus sylvestris*, 4 sample plots of white birch, and 17 sample plots of larch were selected. The plot had high vegetation cover in the forest and sparse understory vegetation. The sites of field sampling plots are shown in Fig. 1(b). The size of each plot was 30 m × 30 m, and the geographic coordinates and dominant tree species of the plot, diameter at breast, and height of all trees

were measured. All the trees in each plot were divided into three sections according to the diameter at breast height from small to large, and three sample trees were randomly selected for each diameter class according to the three diameter classes. One core sample from both sides of the tree was obtained with a 5-mm diameter drill at breast height. In total, 288 cores were collected. The cores were dried, mounted, and gradually sanded to a high polish. After careful cross-dating [32], the calendar year of each tree ring was determined using standard dendrochronological techniques.

Forest NPP is the sum of biomass growth and litter and animal feed intake. Since the Saihanba area is a national nature reserve, it is less affected by human and animal disturbances. In addition, the amount of litter was basically constant after the forest canopy was closed. Therefore, the amount of litter and animal feed intake could be neglected in this study. The height-DBH model of each tree species was established using plot data, and then the annual DBH and tree height were obtained based on tree-ring width data. The annual aboveground biomass was estimated based on the biomass estimation formula of each tree species [33]. Finally, the annual growth of biomass was approximately taken as the annual forest NPP.

4) *DEM Data*: The new Global Digital Elevation Model (GDEM v2) products with a resolution of 30 m came from the Geospatial Data Cloud platform.³ They were generated from ASTER data. In this study, seven DEM images (N40E117, N41E115, N41E116, N41E117, N42E115, N42E116, and N42E117) were collected. Furthermore, the slope data and aspect data were extracted from DEM data.

5) *Forest Aboveground Biomass*: Forest aboveground biomass at a resolution of 30 m, with an R^2 of 0.50 and the root-mean-square error (RMSE) of 30.33 Mg/ha, was estimated based on a random forest model by using the Geoscience Laser Altimeter System (GLAS) data on Ice, Cloud, and land Elevation Satellite (ICESat) and Landsat surface reflectance products.

III. METHODS

To obtain time series of high-resolution GPP/NPP at monthly scale, we combined a downscaling method and an LUE-based NPP model (see Fig. 2). Using Landsat surface reflectance products and GLASS LAI/FPAR products, the downscaling method was adopted to produce monthly high resolution (30 m) LAI/FPAR. Then, the monthly GPP/NPP was calculated with the MuSyQ-NPP model by inputting the land-cover data, forest biomass, meteorological data, and downscaled LAI and FPAR. Ground-based field data were used to validate NPP estimates. In addition, the spatiotemporal variation characteristics of NPP and their relevance with climatic factors were analyzed.

A. Estimation of High-Resolution GPP/NPP

1) *Downscaling of LAI and FPAR*: The spatiotemporal enhancement method for medium-resolution LAI (STEM-LAI) is a downscaling method aimed at generating high-resolution LAI

¹[Online]. Available: <http://www.bnu-datacenter.com/en>

²[Online]. Available: <https://lpcexplorer.cr.usgs.gov/>

³[Online]. Available: <http://www.gscloud.cn>

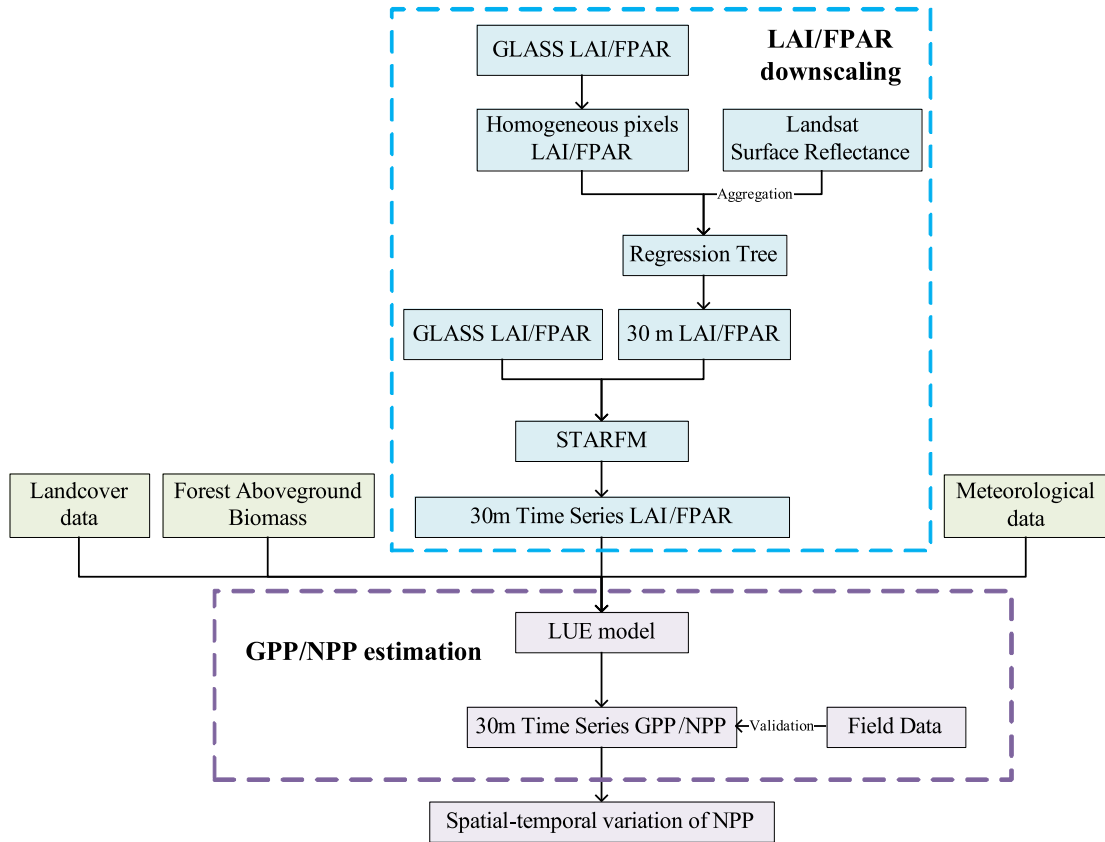


Fig. 2. Flowchart of GPP/NPP estimates from downscaling method and LUE-based NPP model.

from Landsat and MODIS data by combining a regression tree model [34] and Spatial and Temporal Adaptive Reflectance Fusion Model (STARFM) [35]–[38]. In this work, the STEM-LAI was adopted to downscale the 1 km/500 m GLASS LAI/FPAR to 30 m LAI/FPAR.

First, high-quality GLASS LAI/FPAR samples were selected according to product quality flags to ensure the optimum quality of the regression tree training. Then, the coefficients of variation (CV) of Landsat reflectance pixels within each GLASS 1 km or 500 m pixel was computed to select GLASS pure pixels with low heterogeneity according to the threshold. GLASS pixels with the band mean CV below the threshold was recognized to be pure pixels. A cubist regression tree model was built adopting GLASS pure pixels and aggregated Landsat reflectance (1 km/500 m), and then applied to high-resolution (30 m) Landsat reflectance images to obtain high-resolution (30 m) LAI/FPAR.

Finally, STARFM was used for time-series GLASS LAI/FPAR (1 km/500 m) and Landsat-derived high-resolution LAI/FPAR (30 m) to produce time-series high-resolution LAI/FPAR (30 m).

2) *Estimation of GPP/NPP*: The MuSyQ-NPP model was used to obtain 30-m GPP/NPP. MuSyQ-NPP model is an LUE model developed by Cui *et al.* [39]; it adopts the principle of LUE to estimate GPP and NPP is the residual of GPP and autotrophic respiration. The model has been validated by Cui *et al.* [39] and Yu *et al.* [40] in China and globally, and the R^2 and RMSE between estimated NPP and BigFoot NPP were 0.84 and 160.16

Vegetable Types	$\varepsilon_g(\text{gC/MJ})$
Cropland	1.5
Evergreen needle-leaf forest (ENF)	0.962
Deciduous needle-leaf forest (DNF)	1.086
Deciduous broadleaved forest (DBF)	1.165
Mixed forest	1.051
Shrub	0.841
Grassland	0.86
Wetland	0.86

$\text{gC}\cdot\text{m}^{-2}\cdot\text{yr}^{-1}$, which is better than MOD17 NPP products with R^2 and RMSE of 0.55 and 219.26 $\text{gC}\cdot\text{m}^{-2}\cdot\text{yr}^{-1}$ [40]. GPP and NPP could be expressed as follows:

$$\text{GPP} = \varepsilon_g \times \text{FPAR} \times \text{PAR} \times f_1(T) \times f_2(\beta) \quad (1)$$

$$\text{NPP} = \text{GPP} - R_a \quad (2)$$

where ε_g represents the biome-specific potential LUE, which is determined by land-cover type [9], as shown in Table I. FPAR is the fraction of PAR absorbed by vegetation canopy.

$f_1(T)$ and $f_2(\beta)$ are the limited influence of temperature and water conditions on ε_g , respectively. $f_1(T)$ is computed by using the expression in the CASA model [7]. Vapor pressure deficit (VPD) has been used to estimate water press on vegetation productivity in some models, such as MOD17 [9] and the revised EC-LUE model [41]. However, VPD might not fully reflect the effect of water conditions on vegetation growth, especially for the irrigated cropland in an arid or a semiarid area. In the MuSyQ-NPP model, we used the ratio of actual evapotranspiration to potential evapotranspiration to reflect the water press, and $f_2(\beta)$ is expressed as

$$f_2(\beta) = 0.5 + 0.5(E/E_p) \quad (3)$$

where E and E_p are actual and potential evapotranspiration, respectively, and E was calculated by using an improved Penman–Monteith approach and remotely sensed LAI data [42], [43], and E_p was calculated with Priestley–Taylor equation [44]. R_a is autotrophic respiration, which can be expressed as

$$R_a = R_m + R_g = \sum (R_{m,i} + R_{g,i}) \quad (4)$$

$$R_{m,i} = M_i r_{m,i} Q_{10,i}^{(T-T_b)/10} \quad (5)$$

$$R_g = \gamma(GPP - R_m) \quad (6)$$

where R_m and R_g are maintenance respiration and growth respiration, respectively. M_i , $r_{m,i}$, and $Q_{10,i}$ are the live biomass of the plant component, the maintenance respiration coefficient, and the temperature sensitivity factor. T_b and T are the base temperature and the daily average temperature. R_g is the portion to the difference between GPP and R_m . The growth respiration coefficient γ is 0.25.

B. Analysis of Spatiotemporal Variation of NPP

The spatiotemporal trends of NPP in the upper Luanhe River basin were analyzed by the pixel-by-pixel linear regression method [45]. The partial correlation analysis method was used to study the response of NPP to climatic factors, and the relationship between the standardized precipitation index (SPI) and NPP was also analyzed. The partial correlation is calculated as follows:

$$r_{xy,z} = \frac{r_{xy} - r_{xz} \cdot r_{yz}}{\sqrt{(1 - r_{xz}^2)(1 - r_{yz}^2)}} \quad (7)$$

where r_{xy} , r_{xz} , and r_{yz} are the correlation coefficients of variables x and y , x and z , and y and z , respectively. $r_{xy,z}$ is the partial correlation coefficient of the variables x and y after the variable z is fixed.

SPI is a precipitation index, which assumes that the distribution of precipitation is skewed [46]. The SPI has the advantages of multiple time scales, fine spatial consistency, and temporal flexibility [47], and thus has been widely used in the spatiotemporal analysis of drought [48], [49]. To analyze the effect of precipitation on NPP, we also calculated SPI in the study area. The detail of SPI calculation was described in Supplementary Material.

TABLE II
GRADING STANDARD OF DROUGHT DEGREE BY THE SPI

Drought level description	SPI index
No drought	$-0.5 \leq \text{SPI}$
Mild drought	$-1.0 < \text{SPI} \leq -0.5$
Moderate drought	$-1.5 < \text{SPI} \leq -1.0$
Severe drought	$-2.0 < \text{SPI} \leq -1.5$
Serious drought	$\text{SPI} \leq -2.0$

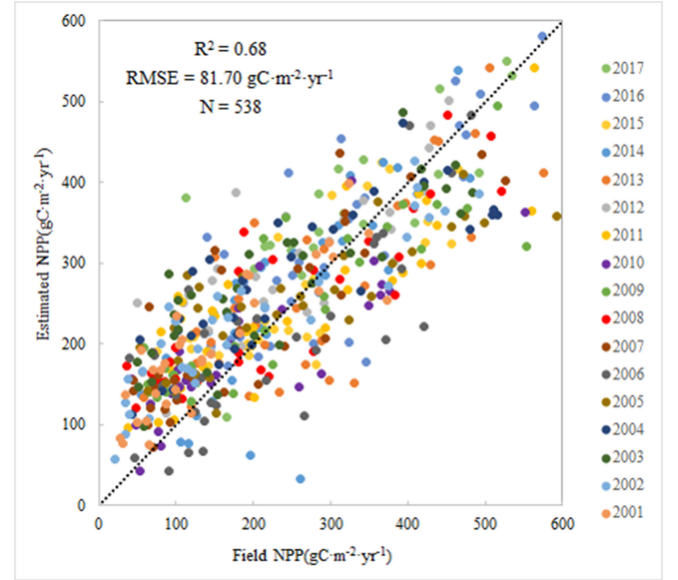


Fig. 3. Validation of estimated NPP against field NPP.

It is commonly believed that a short-term scale SPI (e.g., 3 or 6 months) can better reflect drought-affected vegetation [47]. In this article, the SPI was calculated on a 6-month time scale. The smaller the SPI, the higher the degree of drought, indicating a more severe drought. According to the grading standard of the National Climate Center, China, the drought level can be divided into five levels [50]. The specific grading standards are shown in Table II.

IV. RESULTS

A. Validation of Estimated NPP

We only validated the estimated NPP with field investigated forest NPP data in this article. The scatterplot between the estimated NPP and field NPP data is shown in Fig. 3. There was a remarkable linear relationship between the field NPP and estimated NPP. The RMSE was $81.70 \text{ gC}\cdot\text{m}^{-2}\cdot\text{yr}^{-1}$ and R^2 value was 0.68. The yearly validation results of NPP from 2001 to 2017 were shown in Table III, which showed that the value of RMSE ranged from $66.95 \text{ gC}\cdot\text{m}^{-2}\cdot\text{yr}^{-1}$ to $93.58 \text{ gC}\cdot\text{m}^{-2}\cdot\text{yr}^{-1}$, and the value of R^2 ranged from 0.60 to 0.85. We found that there was an NPP overestimation at low values. One of the reasons for the overestimation could be that litter and animal feed intake were

TABLE III
YEARLY VALIDATION RESULTS OF NPP FROM 2001 TO 2017

year	R ²	RMSE	N
2001	0.76	71.32	31
2002	0.85	77.16	32
2003	0.73	91.25	32
2004	0.67	93.58	32
2005	0.69	93.03	32
2006	0.66	87	32
2007	0.73	76.32	32
2008	0.77	77.1	32
2009	0.8	76.1	32
2010	0.72	77.9	32
2011	0.71	84.31	33
2012	0.73	86.24	33
2013	0.6	86.46	33
2014	0.64	75	33
2015	0.63	66.95	33
2016	0.65	77.55	33
2017	0.6	87.94	21

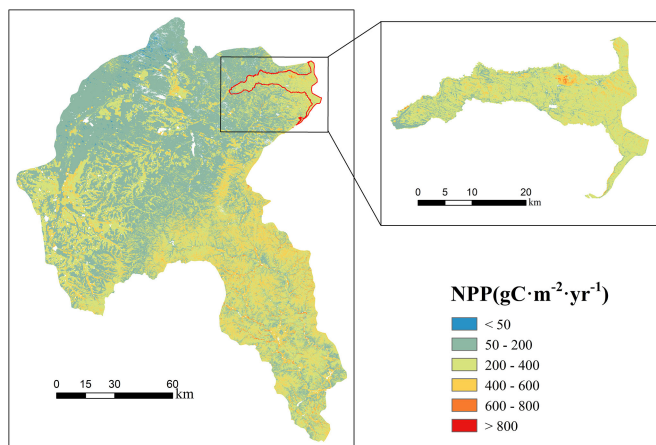


Fig. 4. Average NPP in the upper Luanhe River basin from 2001 to 2017.

not included in the field NPP, which caused the underestimation of field NPP.

B. Spatiotemporal Variation of NPP

The average NPP in the upper Luanhe River catchment from 2001 to 2017 is shown in Fig. 4. NPP in the study area revealed a decreasing pattern from southeast to northwest. High NPP values were mainly distributed in the southeastern and northeastern forest areas and western cropland area, with a range of 200–600 $\text{gC}\cdot\text{m}^{-2}\cdot\text{yr}^{-1}$. Low NPP values were distributed extensively in

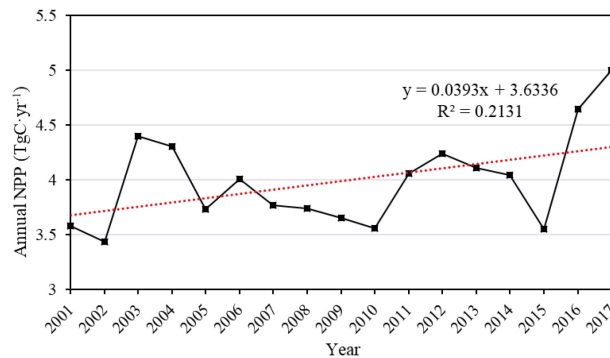


Fig. 5. Interannual variation of total NPP in the upper Luanhe River basin from 2001 to 2017.

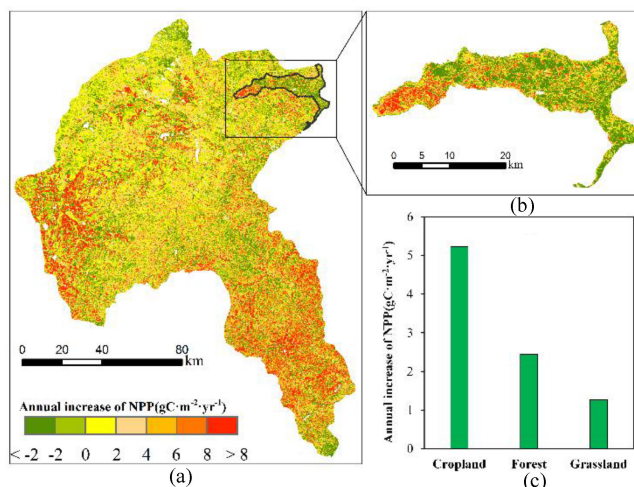


Fig. 6. (a) NPP trends in the upper Luanhe River basin from 2001 to 2017, (b) the NPP trend of Saihanba area, and (c) trends of main vegetation types.

the middle and northern grassland areas, with a range of 50–200 $\text{gC}\cdot\text{m}^{-2}\cdot\text{yr}^{-1}$. NPP values in the Saihanba area were mostly distributed in the range of 200–400 $\text{gC}\cdot\text{m}^{-2}\cdot\text{yr}^{-1}$, and the highest was 704.5 $\text{gC}\cdot\text{m}^{-2}\cdot\text{yr}^{-1}$.

The interannual variation in total NPP in the upper Luanhe River basin from 2001 to 2017 is shown in Fig. 5. Annual NPP had a fluctuating increasing trend from 2001 to 2017, with values ranging between 3.43 and 5.00 $\text{TgC}\cdot\text{yr}^{-1}$ ($1 \text{ Tg} = 1 \times 10^{12} \text{ g}$), with a mean of 3.99 $\text{TgC}\cdot\text{yr}^{-1}$ and an annual increase of 0.04 $\text{TgC}\cdot\text{yr}^{-1}$. The peak NPP was presented in 2017, and the minimum was presented in 2002. However, the changing trend of NPP varied in different time periods. NPP increased significantly in 2002–2003, 2010–2012, and 2015–2017, with an annual growth rate of 0.97 $\text{TgC}\cdot\text{yr}^{-1}$, 0.34 $\text{TgC}\cdot\text{yr}^{-1}$, and 0.81 $\text{TgC}\cdot\text{yr}^{-1}$, respectively. NPP had a fluctuating decreasing trend in 2003–2010 and 2012–2015, with an annual growth rate of $-0.12 \text{ TgC}\cdot\text{yr}^{-1}$ and $-0.23 \text{ TgC}\cdot\text{yr}^{-1}$, respectively.

The slope of NPP obtained by linear regression of NPP in the past 17 years is shown in Fig. 6. The results indicated that NPP presented an upward tendency in most of the study area. The statistics of the trend spatial distribution map of NPP show that NPP increased most significantly in the southeastern

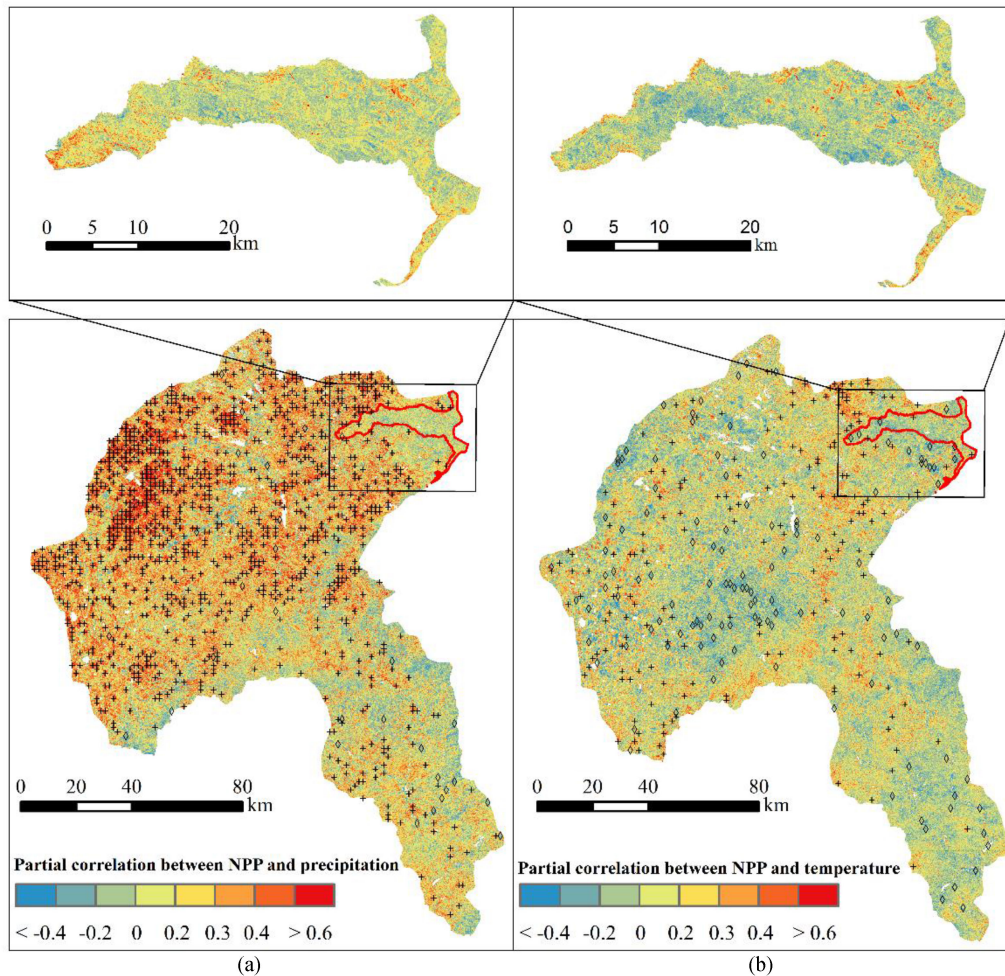


Fig. 7. Partial correlation distribution between annual NPP and (a) total annual precipitation and (b) average annual temperature. + are statistically significant positive correlation ($p \leq 0.05$), and \diamond are statistically significant negative correlation ($p \leq 0.05$).

forest area and western cropland area, with the highest increase of $52.6 \text{ gC}\cdot\text{m}^{-2}\cdot\text{yr}^{-1}$. NPP increased slightly in the central grassland area and decreased in the northeastern forest area and the southernmost forest area, with a lowest increase of $-58.37 \text{ gC}\cdot\text{m}^{-2}\cdot\text{yr}^{-1}$. Among the major land-cover types, farmland had the fastest rate of increase ($5.23 \text{ gC}\cdot\text{m}^{-2}\cdot\text{yr}^{-1}$), secondary by forest ($2.44 \text{ gC}\cdot\text{m}^{-2}\cdot\text{yr}^{-1}$), and the smallest was observed for grassland ($1.27 \text{ gC}\cdot\text{m}^{-2}\cdot\text{yr}^{-1}$). In the Saihanba area, NPP increased obviously in the west but increased insignificantly or decreased slightly in most other areas.

C. Effects of Climatic Factors on Annual NPP Change

Fig. 7 shows the distribution of partial correlations between annual NPP and climatic factors (precipitation and temperature). There was a remarkably positive correlation between NPP and annual precipitation, with 76% of the regions with positive correlation, 14% of the regions with significant positive correlation, and almost none of the regions with significant negative correlation [see Fig. 7(a)]. The strongest correlations between

NPP and precipitation was primarily located in the northwestern farmland and grassland areas, while the correlations in the forest area were poor, which indicated that precipitation had obvious promotional influences on grassland growth in the study area. The partial correlations between annual NPP and average annual temperature based on pixels is shown in Fig. 7(b). The partial correlation between NPP and mean annual temperature was weak. Although the area of positive correlation between temperature and NPP was about 55% of total area, the significant positive correlated area ($p \leq 0.05$) was less than 1%, and the significant negative correlation only accounts for 2% of the study area. The correlations of NPP with temperature and precipitation were not significant in most of the Saihanba area.

As Fig. 8 illustrates, droughts mainly occurred in 2001, early 2006, 2009–2010, and early 2012. NPP in 2001–2002, 2009–2010, and 2015 was low. The drought in 2006 and 2012 appeared in Winter (February and January, respectively), and the drought period is short, which had weak impact on NPP. The moderate drought in 2009–2010 lasted about 6 months, which caused the large decrease in NPP in 2009 and 2010.

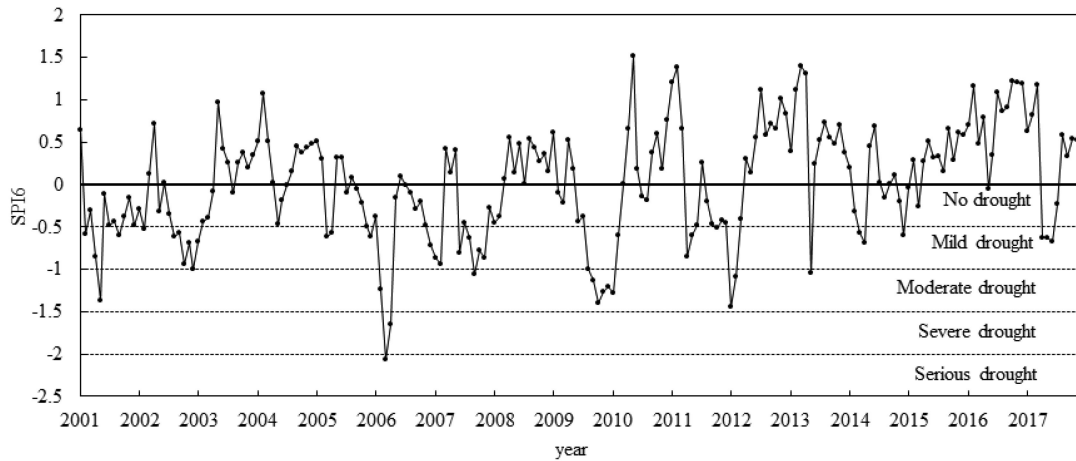


Fig. 8. Temporal variation trends of SPI in the upper Luanhe River basin.

V. DISCUSSION

A. Uncertainties of NPP Simulation

High spatial resolution NPP data are essential for monitoring small- and medium-scale ecosystem carbon cycles. The verification of field forest NPP data showed that this downscaling framework performs well in acquiring time series of NPP data in the upper Luanhe River catchment. However, there are still uncertainties in this study. First, the downscaling process of LAI and FPAR could cause some uncertainties. The accuracy of the cubist regression tree model used in the downscaling process depended on the quantity and quality of training samples, which could affect the quality of high-resolution LAI and FPAR reference images [38], [51]. The pixels of GLASS 1 km/500 m products are mostly mixed because of the spatial heterogeneity, the widely existence of low vegetation cover types (e.g., bare land) could result in the low values of GLASS LAI and FPAR products in the growing season. So, the high values of LAI and FPAR could not be described accurately. Second, limited by the data quality of Landsat surface reflectance products, such as cloud cover, only a single reference high-resolution image in summer for each year was selected to estimate the LAI and FPAR for a year by using STARFM model. However, the closer to the reference date, the more accurate the downscaling results were. The precision of the downscaled LAI and FPAR was limited in the early and late months of a year, such as January to March and October to December [14]. Third, limited by the field experiment, the NPP estimation was only validated by the investigated data from forest samples. The accuracy of NPP for other vegetation types still needed to be done in future.

B. Driving Forces of NPP Change

Temperature and precipitation changes could regulate the hydrothermal conditions for vegetation growth, particularly in dryland ecosystems [52], [16]; therefore, arid and semiarid ecosystems are dramatically susceptible to climate change [53]. In our research, the precipitation in the upper Luanhe River

catchment was positively correlated with NPP, and the correlation between temperature and NPP was weak, suggesting that the changes in NPP were mainly affected by precipitation. Therefore, the upward in precipitation was the important reason for the rise in NPP, and the correlation between temperature and NPP changes is weak, which is in accordance with the results of previous studies in this area [16], [19], [20]. In the agricultural transition zone of northern China, Jiang *et al.* [16] found that only 1% of area temperature was significantly associated with NPP from 2000 to 2015, and only 2% of the region where the temperature was significantly related to NPP in our study area, indicating that the temperature in this region has a weak influence on NPP. Climate warming may have weakened the association between vegetation growth and temperature in the north [54]. Although rising temperatures can extend the growing season of vegetation, they can also lead to an increase in evapotranspiration; thus, the influence of water stress on vegetation growth could increase when the change in precipitation was not obvious. In addition, rising temperatures could increase the autotrophic respiration of vegetation, thus causing a decline in NPP.

NPP responds differently to precipitation under different land-use types, and the association between NPP and grassland is obviously superior to the forest. Forests are greater efficiency at utilizing water than grasslands during drought [17], [21], [22], and most forests can endure water scarcity as they might obtain water contained in the deep soil layers [55]. Grassland phenology and growth conditions are usually more sensitive to precipitation than forests [56].

It is worth noting that the NPP of cropland had a rapid growth trend, and the precipitation also had a strong correlation with NPP. Meanwhile, human activities can adjust the response of cropland NPP to precipitation changes through irrigation and fertilization [17], [57]. Especially in arid and semiarid areas, NPP of agricultural land is generally higher than that of forest and grassland areas with the help of artificial irrigation and other agricultural inputs [58]. The study by Sun *et al.* also found that improved farm production practices, fertilization and irrigation had a significant effect on vegetation productivity in the upper

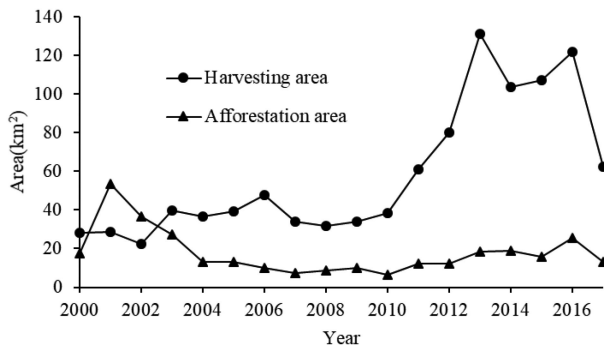


Fig. 9. Trend of harvesting area and afforestation area in the Saihanba forest farm from 2001 to 2017.

Luanhe River basin [59]. Thus, the increase in NPP in cropland is driven by a combination of precipitation and human activities.

In addition to being influenced by climate, the annual variation of NPP in Saihanba area is also influenced by human activities. NPP increased significantly in the western part of the Saihanba, while it increased insignificantly or decreased slightly in most other areas of the Saihanba (see Fig. 6), and the correlation between annual NPP and precipitation or temperature was weak (see Fig. 7), which was also related to forest management. Western Saihanba is mainly located in the core area of the Saihanba National Nature Reserve, and the obvious increase in NPP reflected the significant effect of forest protection and afforestation over the years. For the area outside of the Nature Reserve in the Saihanba area, there were both afforestation and selective cutting of trees. According to the statistics of Saihanba Forest Farm, the cutting area (including tending, excavation, secondary forest transformation, logging, low yield forest improvement, and final cutting) increased from 2001 to 2017, but the afforestation area showed a downward trend, as shown in Fig. 9, which would affect forest density and slow down the increasing trend of NPP and decrease the correlation between NPP and climatic factors.

VI. CONCLUSION

In this article, time-series NPP of 30 m resolution in the upper Luanhe River Basin was generated by the data fusion model and MuSyQ-NPP model. Compared with field forest NPP, we derived an R^2 of 0.68 and RMSE of $81.70 \text{ gC}\cdot\text{m}^{-2}\cdot\text{yr}^{-1}$, which proved that the estimated NPP was reliable and that the combination of the downscaling method and LUE-based NPP model was practicable. High NPP were distributed primarily in the southeastern and northeastern forest areas and western cropland area, and low NPP were distributed extensively in the middle and northern grassland areas. Annual NPP had a fluctuating increasing trend from 2001 to 2017, with values ranging between 3.43 and $5.00 \text{ TgC}\cdot\text{yr}^{-1}$, and an annual upward of $0.04 \text{ TgC}\cdot\text{yr}^{-1}$. The results also showed that precipitation is an important reason for the interannual variation of NPP in the upper Luanhe River basin, and grasslands were more sensitive to precipitation than forests. Human activities, such as forest management, also strongly affect annual changes in NPP, and

the weak relevant between annual NPP and climatic factors in the Saihanba area can also be attributed to afforestation and selective cutting of trees.

REFERENCES

- [1] C. B. Field, M. J. Behrenfeld, J. T. Randerson, and P. Falkowski, "Primary production of the biosphere: Integrating terrestrial and oceanic components," *Science*, vol. 281, no. 5374, pp. 237–240, 1998.
- [2] T. E. Twine and C. J. Kucharik, "Climate impacts on net primary productivity trends in natural and managed ecosystems of the central and eastern United States," *Agric. Forest Meteorol.*, vol. 149, no. 12, pp. 2143–2161, 2009.
- [3] M. Zhao and S. W. Running, "Drought-induced reduction in global terrestrial net primary production from 2000 through 2009," *Science*, vol. 329, no. 5994, pp. 940–943, 2010.
- [4] Y. Wenping, C. Wenwen, L. Dan, and D. Wenjie, "Satellite-based vegetation production models of terrestrial ecosystem: An overview," *Adv. Earth Sci.*, vol. 29, no. 5, pp. 541–550, 2014.
- [5] IGBP Terrestrial Carbon Working Group, "The terrestrial carbon cycle: Implications for the Kyoto Protocol," *Science*, vol. 280, pp. 1393–1394, 1998.
- [6] D. D. Baldocchi, "Assessing the eddy covariance technique for evaluating carbon dioxide exchange rates of ecosystems: Past, present and future," *Global Change Biol.*, vol. 9, no. 4, pp. 479–492, 2003.
- [7] C. S. Potter *et al.*, "Terrestrial ecosystem production: A process model based on global satellite and surface data," *Global Biogeochem. Cycles*, vol. 7, no. 4, pp. 811–841, 1993.
- [8] S. D. Prince and S. N. Goward, "Global primary production: A remote sensing approach," *J. Biogeogr.*, vol. 22, pp. 815–835, 1995.
- [9] S. W. Running and M. Zhao, "Daily GPP and annual NPP (MOD17A2/A3) products NASA earth observing system MODIS land algorithm," *MOD17 User's Guide*, vol. 2015, pp. 1–28, 2015.
- [10] W. Yuan *et al.*, "Deriving a light use efficiency model from eddy covariance flux data for predicting daily gross primary production across biomes," *Agric. Forest Meteorol.*, vol. 143, no. 3/4, pp. 189–207, 2007.
- [11] X. Xiao *et al.*, "Satellite-based modeling of gross primary production in an evergreen needleleaf forest," *Remote Sens. Environ.*, vol. 89, no. 4, pp. 519–534, 2004.
- [12] S. W. Running, R. R. Nemani, F. A. Heinsch, M. Zhao, M. Reeves, and H. Hashimoto, "A continuous satellite-derived measure of global terrestrial primary production," *Bioscience*, vol. 54, no. 6, pp. 547–560, 2004.
- [13] C. M. Gevaert and F. J. García-Haro, "A comparison of STARFM and an unmixing-based algorithm for Landsat and MODIS data fusion," *Remote Sens. Environ.*, vol. 156, pp. 34–44, 2015.
- [14] T. Yu, R. Sun, Z. Xiao, Q. Zhang, J. Wang, and G. Liu, "Generation of high resolution vegetation productivity from a downscaling method," *Remote Sens.*, vol. 10, no. 11, 2018, Art. no. 1748.
- [15] D. Xu, C. Li, X. Song, and H. Ren, "The dynamics of desertification in the farming-pastoral region of North China over the past 10 years and their relationship to climate change and human activity," *CATENA*, vol. 123, pp. 11–22, 2014.
- [16] H. Jiang, X. Xu, M. Guan, L. Wang, Y. Huang, and Y. Jiang, "Determining the contributions of climate change and human activities to vegetation dynamics in agro-pastoral transitional zone of northern China from 2000 to 2015," *Sci. Total Environ.*, vol. 718, 2020, Art. no. 134871.
- [17] H.-J. Xu and X.-P. Wang, "Effects of altered precipitation regimes on plant productivity in the arid region of northern China," *Ecol. Informat.*, vol. 31, pp. 137–146, 2016.
- [18] Y. Yin, H. Deng, and D. Ma, "Complex effects of moisture conditions and temperature enhanced vegetation growth in the arid/humid transition zone in Northern China," *Sci. Total Environ.*, vol. 805, 2022, Art. no. 150152.
- [19] W. Ge, L. Deng, F. Wang, and J. Han, "Quantifying the contributions of human activities and climate change to vegetation net primary productivity dynamics in China from 2001 to 2016," *Sci. Total Environ.*, vol. 773, 2021, Art. no. 145648.
- [20] J. Wang *et al.*, "Decreasing net primary production due to drought and slight decreases in solar radiation in China from 2000 to 2012," *J. Geophys. Res., Biogeosci.*, vol. 122, no. 1, pp. 261–278, 2017.
- [21] L. Y. Huang, Q. L. Yan, T. Gao, and Z. Jiao-Jun, "Estimation on stock volume of plantation forests using ALOS PALSAR images: A case study of Larix principis-rupprechtii plantations in Saihanba forest farm," *Chin. J. Ecol.*, vol. 34, pp. 2401–2409, 2015.

- [22] S. Wolf *et al.*, “Contrasting response of grassland versus forest carbon and water fluxes to spring drought in Switzerland,” *Environ. Res. Lett.*, vol. 8, no. 3, 2013, Art. no. 035007.
- [23] E. Stuart-Haëntjens *et al.*, “Mean annual precipitation predicts primary production resistance and resilience to extreme drought,” *Sci. Total Environ.*, vol. 636, pp. 360–366, 2018.
- [24] S. Mukherjee, A. Mishra, and K. E. Trenberth, “Climate change and drought: A perspective on drought indices,” *Curr. Climate Change Rep.*, vol. 4, no. 2, pp. 145–163, 2018.
- [25] S. Liang *et al.*, “A long-term global Land surface satellite (GLASS) data-set for environmental studies,” *Int. J. Digit. Earth*, vol. 6, no. suppl, pp. 5–33, 2013.
- [26] Z. Xiao *et al.*, “Use of general regression neural networks for generating the GLASS leaf area index product from time-series MODIS surface reflectance,” *IEEE Trans. Geosci. Remote Sens.*, vol. 52, no. 1, pp. 209–223, Jan. 2014.
- [27] Z. Xiao, S. Liang, J. Wang, Y. Xiang, X. Zhao, and J. Song, “Long-time-series global land surface satellite leaf area index product derived from MODIS and AVHRR surface reflectance,” *IEEE Trans. Geosci. Remote Sens.*, vol. 54, no. 9, pp. 5301–5318, Sep. 2016.
- [28] Z. Xiao, S. Liang, R. Sun, J. Wang, and B. Jiang, “Estimating the fraction of absorbed photosynthetically active radiation from the MODIS data based GLASS leaf area index product,” *Remote Sens. Environ.*, vol. 171, pp. 105–117, 2015.
- [29] J. Chen, X. Cao, S. Peng, and H. Ren, “Analysis and applications of GlobeLand30: A review,” *ISPRS Int. J. Geo-Inf.*, vol. 6, no. 8, 2017, Art. no. 230.
- [30] C. Li *et al.*, “A Circa 2010 thirty meter resolution forest map for China,” *Remote Sens.*, vol. 6, no. 6, pp. 5325–5343, 2014.
- [31] R. D. Hungerford, R. R. Nemani, S. W. Running, and J. C. Coughlan, “MTCLIM: A mountain microclimate simulation model,” U.S. Dept. Agriculture, Forest Service, Intermountain Res. Station, INT-RP-414, 1989.
- [32] E. R. Cook and L. Kairiukstis, *Methods of Dendrochronology*. Dordrecht, The Netherlands: Springer, 1990.
- [33] W. X. Luo and Y. Lu F, *Handbook of Biomass Model For Main Forest Trees in China*. Beijing, China: China Forestry Publishing House, 2015.
- [34] R. Houborg, M. F. McCabe, and F. Gao, “A spatio-temporal enhancement method for medium resolution LAI (STEM-LAI),” *Int. J. Appl. Earth Observ. Geoinf.*, vol. 47, pp. 15–29, 2016.
- [35] P. Wang, F. Gao, and J. G. Masek, “Operational data fusion framework for building frequent landsat-like imagery,” *IEEE Trans. Geosci. Remote Sens.*, vol. 52, no. 11, pp. 7353–7365, Nov. 2014.
- [36] C. Cammalleri, M. Anderson, F. Gao, C. Hain, and W. Kustas, “Mapping daily evapotranspiration at field scales over rainfed and irrigated agricultural areas using remote sensing data fusion,” *Agric. Forest Meteorol.*, vol. 186, pp. 1–11, 2014.
- [37] Q. Weng, P. Fu, and F. Gao, “Generating daily land surface temperature at Landsat resolution by fusing Landsat and MODIS data,” *Remote Sens. Environ.*, vol. 145, pp. 55–67, 2014.
- [38] F. Gao, M. C. Anderson, W. P. Kustas, and Y. Wang, “Simple method for retrieving leaf area index from Landsat using MODIS leaf area index products as reference,” *J. Appl. Remote Sens.*, vol. 6, no. 1, 2012, Art. no. 063554.
- [39] T. Cui *et al.*, “Estimating vegetation primary production in the Heihe River Basin of China with multi-source and multi-scale data,” *PLoS One*, vol. 11, no. 4, 2016, Art. no. e0153971.
- [40] T. Yu *et al.*, “Estimation of global vegetation productivity from global land surface satellite data,” *Remote Sens.*, vol. 10, no. 2, 2018, Art. no. 327.
- [41] Y. Zheng *et al.*, “Improved estimate of global gross primary production for reproducing its long-term variation, 1982–2017,” *Earth Syst. Sci. Data*, vol. 12, no. 4, pp. 2725–2746, 2020.
- [42] K. Zhang, J. S. Kimball, Q. Mu, L. A. Jones, S. J. Goetz, and S. W. Running, “Satellite based analysis of northern ET trends and associated changes in the regional water balance from 1983 to 2005,” *J. Hydrol.*, vol. 379, no. 1/2, pp. 92–110, 2009.
- [43] C. Qiao *et al.*, “A study of shelterbelt transpiration and cropland evapotranspiration in an irrigated area in the middle reaches of the Heihe River in northwestern China,” *IEEE Geosci. Remote Sens. Lett.*, vol. 12, no. 2, pp. 369–373, Feb. 2015.
- [44] C. H. B. Priestley and R. J. Taylor, “On the assessment of surface heat flux and evaporation using large-scale parameters,” *Monthly Weather Rev.*, vol. 100, no. 2, pp. 81–92, 1972.
- [45] C. Diao, Y. Liu, L. Zhao, G. Zhuo, and Y. Zhang, “Regional-scale vegetation-climate interactions on the Qinghai-Tibet Plateau,” *Ecol. Inform.*, vol. 65, 2021, Art. no. 101413.
- [46] T. B. McKee, N. J. Doesken, and J. Kleist, “The relationship of drought frequency and duration to time scales,” in *Proc. 8th Conf. Appl. Climatol.*, 1993, vol. 17, no. 22, pp. 179–183.
- [47] G. Buttafuoco, T. Caloiero, and R. Coscarelli, “Analyses of drought events in Calabria (Southern Italy) using standardized precipitation index,” *Water Resour. Manage.*, vol. 29, no. 2, pp. 557–573, 2015.
- [48] I. Livada and V. Assimakopoulos, “Spatial and temporal analysis of drought in Greece using the Standardized Precipitation Index (SPI),” *Theor. Appl. Climatol.*, vol. 89, no. 3, pp. 143–153, 2007.
- [49] W. Huang *et al.*, “Evolution characteristics of seasonal drought in the south of China during the past 58 years based on standardized precipitation index,” *Trans. Chin. Soc. Agric. Eng.*, vol. 26, no. 7, pp. 50–59, 2010.
- [50] Q. Liu *et al.*, “SPI-based drought simulation and prediction using ARMA-GARCH model,” *Appl. Math. Comput.*, vol. 355, pp. 96–107, 2019.
- [51] T. Yu, Q. Zhang, and R. Sun, “Comparison of machine learning methods to up-scale gross primary production,” *Remote Sens.*, vol. 13, no. 13, 2021, Art. no. 2448.
- [52] C. Chen *et al.*, “China and India lead in greening of the world through land-use management,” *Nature Sustain.*, vol. 2, no. 2, pp. 122–129, 2019.
- [53] T. Chen *et al.*, “Disentangling the relative impacts of climate change and human activities on arid and semiarid grasslands in Central Asia during 1982–2015,” *Sci. Total Environ.*, vol. 653, pp. 1311–1325, 2019.
- [54] S. Piao *et al.*, “Evidence for a weakening relationship between interannual temperature variability and northern vegetation activity,” *Nature Commun.*, vol. 5, no. 1, pp. 1–7, 2014.
- [55] K. Ogle and J. F. Reynolds, “Plant responses to precipitation in desert ecosystems: Integrating functional types, pulses, thresholds, and delays,” *Oecologia*, vol. 141, no. 2, pp. 282–294, 2004.
- [56] X. Geng *et al.*, “Extended growing season reduced river runoff in Luanhe River basin,” *J. Hydrol.*, vol. 582, 2020, Art. no. 124538.
- [57] M. Valipour, “A comprehensive study on irrigation management in Asia and Oceania,” *Arch. Agronomy Soil Sci.*, vol. 61, no. 9, pp. 1247–1271, 2015.
- [58] X. Xiao *et al.*, “Response of net primary production to land use and climate changes in the middle-reaches of the Heihe River basin,” *Ecol. Evol.*, vol. 9, no. 8, pp. 4651–4666, 2019.
- [59] B. Sun *et al.*, “Identification and assessment of the factors driving vegetation degradation/regeneration in drylands using synthetic high spatiotemporal remote sensing Data—A case study in Zhenglanqi, Inner Mongolia, China,” *Ecol. Indicators*, vol. 107, 2019, Art. no. 105614.



Qinru Liu received the M.Sc. degree in cartography and geographic information system from Beijing Normal University, Beijing, China, in 2020.

Her research interests include using remote sensing data to estimate vegetation productivity.



Liang Zhao is currently working toward the Ph.D. degree in cartography and geographic information systems from Beijing Normal University, Beijing, China.

His research interests include vegetation productivity and chlorophyll fluorescence remote sensing.



Rui Sun received the B.S. degree in agrometeorology from Nanjing Institute of Meteorology, Nanjing, China, in 1992, the M.S. degree in applied meteorology from the Graduate School, Chinese Academy of Agriculture Sciences, Beijing, China, in 1995, and the Ph.D. degree in physical geography from Beijing Normal University, Beijing, China, in 1998.

His research interests include regional net primary productivity estimation, evapotranspiration estimation, and drought monitoring.



Tao Yu received the M.Sc. degree from Renmin University of China, Beijing, China, in 2015, and the Ph.D. degree in geographic information system from Beijing Normal University, Beijing, China, in 2019.

His research interests include remote sensing modeling and applications in forestry, vegetation productivity, scale effects, and scaling methods.



Anran Zhu received the M.Sc. degree in geographic information system from Beijing Normal University, Beijing, China, in 2020.

She is currently with the Xuzhou Economic and Technological Development Zone, Jiangsu Province, China. Her research interests include estimation of light use efficiency of vegetation with remote sensing data.



Shun Cheng received the B.Sc. degree in forestry from Hebei Agricultural University, Baoding, China, in 1995.

He is currently the Director of the Scientific Research Institute of Saihanba Mechanical Forest Farm, Chengde, China. He is mainly engaged in forestry technology research and promotion, such as forest cultivation, forest management, forest certification, basic forestry research, introduction of advanced theories, and promotion of special technologies.



Qi Li received the M.Sc. degree in cartography and geographic information systems from Beijing Normal University, Beijing, China, in 2021.

She is currently with Beijing Municipal Ecological and Environmental Monitoring Center, Beijing, China. Her research interests include estimation of net primary production with remote sensing data.



Mengjia Wang received the M.Sc. degree in cartography and geographic information systems from Beijing Normal University, Beijing, China, in 2018. She is currently working toward the Ph.D. degree in geographic information system with Beijing Normal University, Beijing, China.

Her research interests include vegetation productivity and biomass estimation, and vegetation parameter inversion from passive microwave remote sensing data.